

Filtering Spin and Orbital Moment in Centrosymmetric Systems

Luciano Jacopo D’Onofrio,¹ Maria Teresa Mercaldo,² Wojciech Brzezicki,^{3,4}
Adam Kłosiński,⁴ Federico Mazzola,⁵ Carmine Ortix,² and Mario Cuoco¹

¹*CNR-SPIN, c/o Università di Salerno, IT-84084 Fisciano (SA), Italy*

²*Dipartimento di Fisica “E. R. Caianiello”, Università di Salerno, IT-84084 Fisciano (SA), Italy*

³*Institute of Theoretical Physics, Jagiellonian University,
ulic, S. Łojasiewicza 11, PL-30348 Kraków, Poland*

⁴*International Research Centre MagTop, Institute of Physics,
Polish Academy of Sciences, Aleja Lotników 32/46, PL-02668 Warsaw, Poland*

⁵*CNR-SPIN, c/o Complesso di Monte S. Angelo, IT-80126 Napoli, Italy*

The control of spin and orbital angular momentum without relying on magnetic materials is commonly accomplished by breaking of inversion symmetry, which enables charge-to-spin conversion and spin selectivity in electron transfer processes occurring in chiral media. In contrast to this perspective, we show that orbital moment filtering can be accomplished in centrosymmetric systems: the electron states can be selectively manipulated allowing for the preferential transfer of electrons with a particular orbital momentum orientation. We find that orbital moment filtering is indeed efficiently controlled through orbital couplings that break both mirror and rotational symmetries. We provide the symmetry conditions required for the electron transmission medium to achieve orbital filtering and relate them to the orientation of the orbital moment. The presence of atomic spin-orbit interaction in the centrosymmetric transmission medium leads to the selective filtering of spin and orbital moments. Our findings allow to identify optimal regimes for having highly efficient simultaneous spin and orbital moment filtering.

A key factor in the progress of spintronics and spin-orbitronics, as well as in the development of new functionalities in solid materials, is the capacity to encode, manipulate, and store information using spin and orbital angular momentum. A promising and widely utilized approach for designing spin functionalities and facilitating charge-to-spin conversion involves strong spin-orbit coupling and acentric materials. The spin-momentum locking [1, 2] allows for the control of the spin angular momentum by transforming, for instance, an unpolarized charge current into a spin density and transverse spin current through Edelstein and spin Hall effects [3–8]. It has recently been discovered that many spin-related phenomena can be traced back to orbital mechanisms [9] even without the presence of atomic spin-orbit coupling. In this context, orbital-based couplings can give rise to orbital Hall [10–16], orbital Edelstein [17–21], inverse orbital Edelstein effects [22], orbital photocurrents [23], and orbital sources of Berry curvature [24, 25].

In systems with weak spin-orbit coupling when inversion symmetry breaking occurs alongside the absence of other crystalline symmetries, as seen in chiral structures, other effects can emerge and electron transmission demonstrates selective filtering based on the spin of the electrons. This effect, referred to as chiral induced spin selectivity (CISS), arises from the polarization of electron spins by chiral molecules [26, 27]. Although CISS has primarily been observed in chiral molecules, studies have revealed that chiral crystals can also generate spin-polarized states through the injection of charge currents [28–30]. Despite several investigations there is no consensus on the mechanisms behind the CISS. However, orbital texture and orbital polarization effects have been

proposed to induce spin-polarization both in chiral systems but also in achiral materials that, however, lack a center of inversion [31].

All of these observations indicate that breaking inversion symmetry, along with the presence of spin and orbital textures in momentum space, plays a crucial role for controlling electron spin and orbital moments. Nevertheless, there are certain cases where orbital dynamics [32] and hidden spin polarization can arise in centrosymmetric systems [33, 34] or spin-filtering is achieved with centrosymmetric molecules [35]. Therefore, understanding the mechanisms that enable the manipulation and control of spin and orbital moments from a symmetry perspective is essential.

In this Letter, we address this fundamental issue by exploring how spin and orbital moment filtering can take place in centrosymmetric systems. By utilizing orbital couplings that preserve inversion symmetry and break both mirror and rotational symmetries, we demonstrate the selective transfer of electrons with a specific orientation of orbital momentum. Our findings reveal the connection between symmetry-breaking interactions and the manipulation of the orbital moment orientation for the transmitted electronic states. Consequently, spin filtering can be realized by introducing a non-zero atomic spin-orbit coupling (SOC) in the centrosymmetric transmission medium. Our analysis indicates the path to achieve high efficiency filtering in the generation of both spin- and orbitally polarized currents by injecting unpolarized electrons into a centrosymmetric medium that lacks mirror and rotational symmetry (Fig. 1).

To illustrate how electron transmission in a centrosymmetric medium that is time-reversal preserving can se-

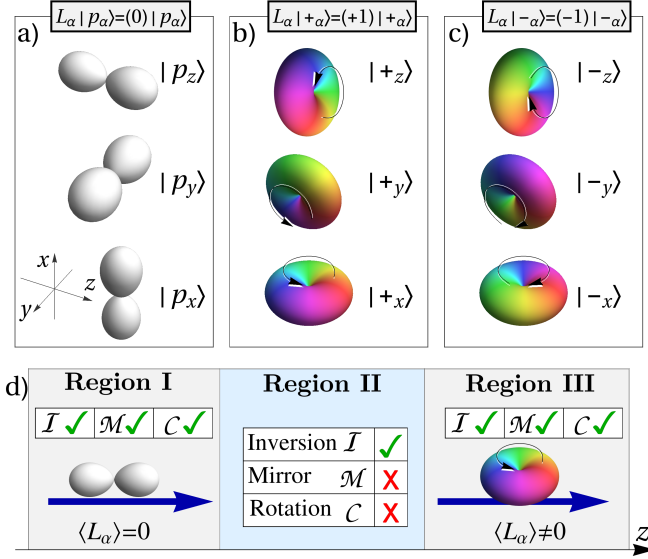


FIG. 1. Schematic of the orbital configurations involved in the transmission process along a given direction (z). Illustration of atomic orbitals $\{|p_z\rangle, |p_y\rangle, |p_x\rangle\}$ having zero (a) and nonvanishing (b),(c) projections of the orbital moment along the x, y, z symmetry directions. Sketch of (b) $+1$ and (c) -1 orbitally polarized configurations. Clockwise or anticlockwise arrows are used to label states with opposite orbital moment along a given direction. $|\pm z\rangle = \frac{1}{\sqrt{2}}(\mp i|p_x\rangle + |p_y\rangle)$ and similarly for the other components. (d) Illustration of electron transmission: An electron is initialized in a state with zero orbital moment in I with preserved inversion (\mathcal{I}), mirror (\mathcal{M}) and rotational (\mathcal{C}) symmetries. It is then transmitted through region II, where \mathcal{M} and \mathcal{C} are broken, before entering region III that has the same symmetry properties of I. The resultant state in III exhibits a non-zero orbital moment.

lectively filter spin and orbital moments, we examine an $L = 1$ multi-orbital electronic system and incorporate orbital couplings to address the breaking of both mirror and rotational symmetries. The electronic states are expressed in terms of atomic orbitals $\{|p_z\rangle, |p_y\rangle, |p_x\rangle\}$. In this manifold, the orbital moment components, \hat{L}_i ($i = x, y, z$), have the standard matrix representation with purely imaginary off-diagonal elements (see Supplemental Material (SM) [36]). For the spin angular momentum, we use the standard representation with $\hat{S}_i = \frac{1}{2}\hat{\sigma}_i$, and $\hat{\sigma}_i$ being the Pauli matrices. The orbital configurations of the electronic states can be also characterized in terms of the products of orbital moment. Given that the orbital angular momentum has pseudovector characteristics with magnetic dipole properties, their nontrivial combination can be classified as an orbital quadrupole. For convenience and clarity we consider a transmission system featuring a single propagation direction (z) and comprises three regions, each exhibiting distinct symmetry characteristics (Fig. 1d). The outer regions (I and III) preserve inversion, mirror and twofold rotational

symmetries. Instead, in the region II we introduce orbital couplings that break only mirror and rotation while keeping inversion symmetry. Hence, the Hamiltonian can be generally expressed as $\hat{\mathcal{H}} = \hat{\mathcal{H}}(z)$:

$$\hat{\mathcal{H}}(z) = \begin{cases} \hat{\mathcal{H}}^I(z) & z < -d/2 \\ \hat{\mathcal{H}}^{II}(z) & -d/2 \leq z \leq d/2 \\ \hat{\mathcal{H}}^{III}(z) & z > d/2 \end{cases}, \quad (1)$$

where d is the width of the region II. The Hamiltonian in II is then given by

$$\hat{\mathcal{H}}^{II}(z) = \hat{p}_z^2 \left(\sum_{i=x,y,z} a_i^{II} \hat{L}_i^2 + \mathbf{g} \cdot \hat{\chi} \right) + \sum_{i=x,y,z} \Delta_i^{II} \hat{L}_i^2 + \mathbf{g}_0 \cdot \hat{\chi}, \quad (2)$$

$$(3)$$

where \hat{p}_z is the electronic linear momentum operator along the z -axis and the terms proportional to \hat{L}_i^2 are crystal fields that preserve mirror, twofold rotation and inversion symmetry. \mathbf{g} , \mathbf{g}_0 are the strength of the orbital couplings that break mirror and rotational symmetries with respect to the x, y, z reference axes. These symmetry breaking interactions are expressed through the operators $\hat{\chi} = (\hat{\chi}_x, \hat{\chi}_y, \hat{\chi}_z)$ with $\hat{\chi}_x = \hat{L}_y \hat{L}_z + \hat{L}_z \hat{L}_y$, and the other components obtained by cyclic index permutation. Both \mathbf{g} and \mathbf{g}_0 can lower the symmetry while preserving the spatial inversion: \mathbf{g} acts through a change in the electron mass, while \mathbf{g}_0 is a crystalline field potential. Since we are dealing with a one-dimensional transmission, the relevant rotation symmetry is the twofold \hat{C}_2 transformation that rotates by π around a given axis. Furthermore, we define the symmetry transformation $\hat{\mathcal{M}}_i$ as the mirror operation relative to the plane that is perpendicular to the i -axis and passing through the origin. We recall that the inversion symmetry is expressed as $\hat{\mathcal{I}} = \hat{\mathcal{M}}_i \hat{C}_{2i}$. Considering that the components of $\hat{\mathbf{L}}$ transform as pseudovectors upon mirror transformation, one can immediately show that the term $\hat{\chi}_x$ preserves $\hat{\mathcal{I}}$ as well as $\hat{\mathcal{M}}_x$ and the twofold rotational symmetry \hat{C}_{2x} with respect to the x -axis. Similar considerations apply to $\hat{\chi}_y$ and $\hat{\chi}_z$. For convenience and clarity we present results with vanishing \mathbf{g}_0 as it does not alter the qualitative behavior of the outcome (see SM [36]). The Hamiltonian in I and III has vanishing \mathbf{g} couplings and, for clarity, we assume that there is no crystal field potential. Splitting of the orbital degeneracy due to Δ_i^{II} , along with mass anisotropy given by a_i^{II} , does not affect the qualitative nature of the results (see SM [36]).

The transmission problem is then analyzed in the standard way by solving the Schrödinger equation in the three regions and imposing proper boundary conditions at their interfaces (see SM [36]). We assume that the initial state (ϕ_{in}) is set up in a configuration with specific orbital occupation corresponding to the zero orbital moment p_x ,

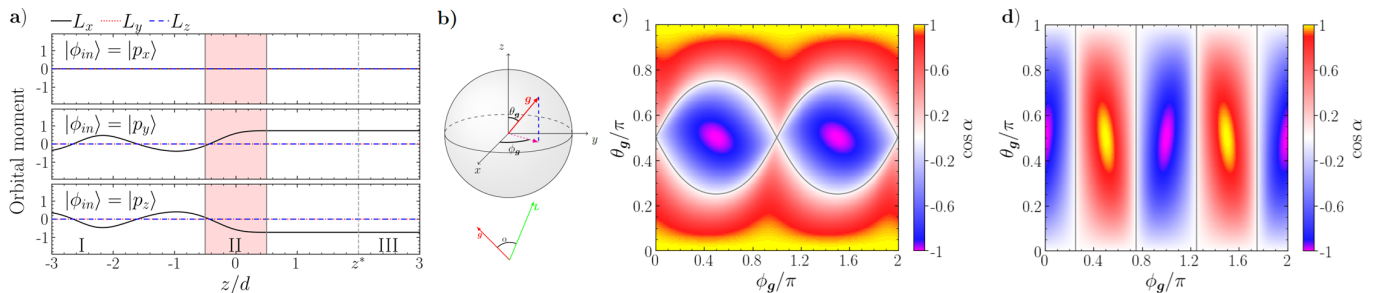


FIG. 2. (a) Spatial profile of the orbital moment associated to the resulting state of the electron transmission problem in the regions I, II (pink shaded area), III, considering different p -orbital configurations as input configurations ($|\phi_{in}\rangle$). (b) Illustration of the spherical parametrization, through the variables (θ_g, ϕ_g) , of the \mathbf{g} -vector coupling in the region II that breaks mirror and rotational symmetries while keeping the inversion symmetry. The angle α is introduced to evaluate the orientation of the orbital moment filtered in the region III with respect to the character of the \mathbf{g} coupling. The evaluation of \mathbf{L} for the outgoing state refers to a given position z^* in the region III as indicated in the panel (a). Contour maps of $\cos \alpha$ for an input state with p_x (c) and p_z (d) type. Solid lines indicate the values of \mathbf{g} coupling for which \mathbf{g} is perpendicular to \mathbf{L} . The results indicate that \mathbf{g} and \mathbf{L} are never collinear except for distinct points corresponding to the single-component \mathbf{g} .

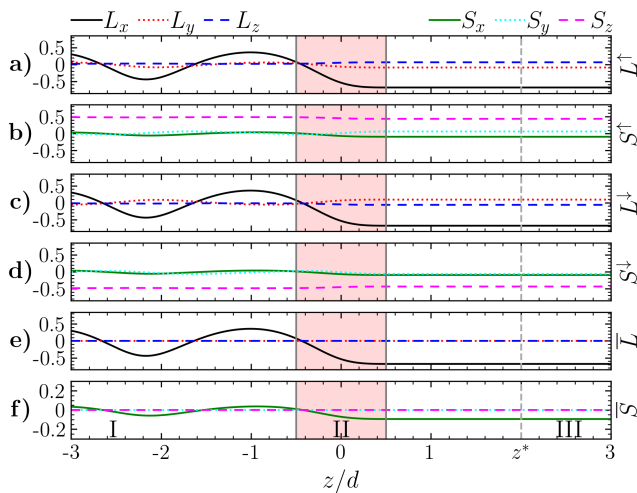


FIG. 3. Spatial profile of orbital ((a) L_\uparrow and (c) L_\downarrow) and spin ((b) S_\uparrow and (d) S_\downarrow) moments associated to the resulting state of the electron transmission problem in the regions I, II (pink shaded area), III, considering a p_z -orbital configuration as input ($|\phi_{in}\rangle$) and spin states with polarization oriented along the z -axis, i.e. $|\uparrow_z\rangle$ and $|\downarrow_z\rangle$. The parameters are $g_x = 0.5$, $g_y = g_z = 0$, and $\lambda/\epsilon_0 = 1$. In panels (e) and (f) we report the spatial profile of $\bar{L} = (L^\uparrow + L^\downarrow)/2$ and $\bar{S} = (S^\uparrow + S^\downarrow)/2$, averaging over the two spin channels considering that the electrons are prepared as an equal mixture of spin up and down configurations: a spin unpolarized charge current is injected into the region II and converted into a spin and orbitally polarized current with net moment oriented along the x -axis.

p_y , and p_z states. The aim is to assess whether there is a probability to transmit an electron with non zero orbital moment in the region III. In order to visualize the character of the transmitted electron current, it is convenient to evaluate the spin and orbital moment polarization at any given position z which is expressed as

$\mathbf{A}(z) = (A_x(z), A_y(z), A_z(z))$ with $A = L, S$ being the orbital and spin moment, respectively. All the outcomes are expressed in terms of a characteristic length scale k_0 and energy $\epsilon_0 = \hbar^2 k_0^2 / 2m$, such that $k_0 d = 1$, with \hbar the reduced Planck constant and m the electron mass, respectively. Moreover, we consider one representative case for the energy μ of the electronic state, i.e. $\mu/\epsilon_0 = 2$. A change in μ does not alter the qualitative behavior of the results.

Let us now examine the electron transmission. We consider a representative case where only one component (e.g. g_x) of the \mathbf{g} couplings is nonzero and the regions I and III have equal electronic parameters so that inversion symmetry holds for the global system too. In this configuration, when ϕ_{in} in region I exhibits only p_x character, the operator $\hat{\chi}_x$ is ineffective. As a result, there is no orbital mixing during propagation, and the outgoing state retains a zero orbital momentum (Fig. 2a). Instead for ϕ_{in} prepared in an orbital configuration of p_y or p_z type, we observe that the probability of obtaining a state with orbital polarization $+x$ differs from that of $-x$ in the outgoing configuration. This leads to a non-zero orbital moment L_x for the transmitted state (see Fig. 2a). One can analytically determine the transmission matrix (see SM [36]) and show the conversion from p_y to states with nonvanishing orbital moment. These results are among the key outcomes of our study, as they illustrate the orbital moment being filtered through a centrosymmetric medium that maintains at least one mirror and a twofold rotational symmetry. We note that inversion symmetry prohibits the presence of a uniform orbital moment in response to the injected current within the system. However, as just demonstrated, it does not eliminate the possibility of having a finite spatial gradient of the orbital moment in response to a charge current.

Now, a question arises of how the orientation of the filtered moment relates to the orbital couplings that gov-

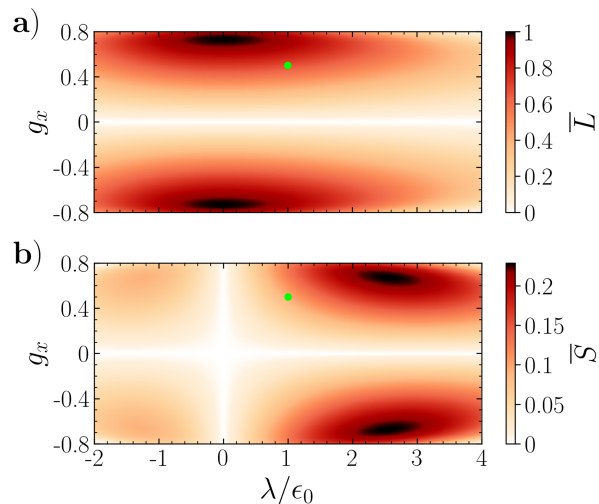


FIG. 4. Average orbital (a) and spin (b) moment across the two spin channels at a specific point in the region III (i.e. z^* in Fig. 3) within (g_x, λ) phase space. Electrons are prepared in a p_z orbital state as an equal mixture of spin up and down configurations aligned along the z -axis. Here, $g_y = g_z = 0$ and the green point corresponds to the values reported in Fig. 3e,f. The profiles of the filtered orbital and spin moments within the (g_x, λ) phase space indicate that the peak amplitudes for the orbital and spin channels arise from distinct configurations.

ern the overall breaking of mirror and rotational symmetries. To achieve this, we set a given amplitude for the \mathbf{g} coupling and use a spherical representation for the (g_x, g_y, g_z) components (Fig. 2b). Next, we determine how the orbital moment in region III correlates with the orbital coupling by calculating the relative angle α between the orbital direction \mathbf{L} of the outgoing state and the \mathbf{g} -vector (Fig. 2b). The results are reported in Fig. 2c,d for an input state with p_x and p_z type (p_y yields behavior analogous to that for p_x) and for a given position z^* in III. The orbital moment filtering ensures that the \mathbf{g} -vector and \mathbf{L} are never collinear, except at specific points where a single component of the \mathbf{g} -vector coupling is considered (Figs. 2c,d). Indeed, if all mirror and twofold rotational symmetries are broken in centrosymmetric region II, the orbital moment of the transmitted electron can change from a collinear to an anticollinear configuration by adjusting either the out-of-plane (g_z) or in-plane orbital couplings (g_x, g_y) in the parameters space. This leads to scenarios where the orbital moment is perpendicular to the \mathbf{g} -vector. These physical configurations have a distinct profile in the \mathbf{g} -parameters space highlighted by solid lines in Figs. 2c,d. The corresponding lines are robust to a change in the amplitude of the model parameters far as the mirror symmetry in the orbital space holds by exchanging two components of the orbital operator $\hat{\mathbf{L}}$ (see SM [36] for details).

Let us then consider the influence of atomic SOC in

the region II expressed through the term $\lambda \hat{\mathbf{L}} \cdot \hat{\mathbf{S}}$. The introduction of the SOC does not alter the symmetry characteristics of the transmission medium. We analyze the electron transmission problem by considering input states that are spin polarized either up or down with respect to a specified direction. In a manner similar to orbital momentum filtering, we then evaluate the outgoing states and the probabilities for each spin channel to be transferred through the region II. The findings are illustrated in Fig. 3 for a specific value of λ , under the assumption that only one component of the \mathbf{g} -coupling is active. In this configuration, the presence of SOC results in non-zero values for both spin and orbital projected polarization, regardless of the orientation (Fig. 3a,b,c,d). By averaging the amplitude of the orbital and spin polarization, respectively, in each direction and taking into account an unpolarized mixture of spin channels for the injected electrons, we observe that the resulting filtering is effective solely for L_x (Fig. 3e) and S_x (Fig. 3f). This is expected since the orbital moment filtering is able to polarize only one component and, due to the structure of the SOC, the corresponding spin polarization gets activated too.

Finally, we examine the quantitative behavior related to spin and orbital moment filtering. To achieve this, we investigate the parameter space of the \mathbf{g} -orbital coupling and the spin-orbit interaction λ (see Fig. 4). For simplicity, we focus solely on the single-component scenario for the \mathbf{g} -coupling. The breaking of all mirror and rotational symmetries in the region II primarily affects the orientation rather than the amplitude of the filtering effect. We observe that the orbital moment increases with the rise in the strength of the symmetry-breaking coupling, yet it reaches its peak when the spin-orbit coupling is negligible. Conversely, the amplitude of the spin moment is optimized through a favorable combination of atomic spin-orbit coupling and orbital interaction that breaks mirror-rotational symmetry. Consequently, the resulting profile exhibits a non-monotonic behavior in the parameter space defined by (g_x, λ) .

In conclusion, our results demonstrate that the breaking of mirror and rotational symmetries—rather than inversion symmetry—is essential for effective spin and orbital filtering, as well as for controlling the orientation of the transmitted angular momentum. Regarding the phenomenon of chiral-induced spin selectivity, the uncovered mechanisms indicate that these effects can also manifest in achiral molecules that possess inversion symmetry along with at least one mirror plane and a twofold rotational symmetry axis. A direct application of our prediction is provided by the use of vanadocene or similar types of molecules [35]. Additionally, our investigation of the role of atomic SOC reveals that, when examining electrical transport with metallic leads connected to the transmission medium, it is not essential for the leads to consist of heavy elements with substantial SOC

[31, 37, 38]. The capability for spin and orbital filtering does not depend on SOC in the areas where charge current is injected or collected, consistently with recent experimental observations [39]. This approach extends beyond molecules, applying for instance to the family of monoclinic and triclinic centrosymmetric materials, or to quasi one-dimensional semiconducting nanostructures [40] with electronic states marked by multiple orbital degrees of freedom.

Acknowledgements

L.J.D'O. and M.C. acknowledge support from PNRR MUR project PE0000023-NQSTI. C.O. and M.T.M. acknowledge partial support by PNRR MUR project PE0000023-NQSTI (TOPQIN) and by the Italian Ministry of Foreign Affairs and International Cooperation, Grants No. PGR12351 (ULTRAQMAT). F.M. acknowledges the PNRR project NFFA-DI, IR0000015. W.B. and A.K. acknowledge support by Narodowe Centrum Nauki (NCN, National Science Centre, Poland) Project No. 2019/34/E/ST3/00404. We acknowledge valuable discussions with Jeroen van den Brink and Panagiotis Kotetes.

-
- [1] E. Rashba, Properties of semiconductors with an extremum loop. i. cyclotron and combinational resonance in a magnetic field perpendicular to the plane of the loop, *Sov. Phys.-Solid State* **2**, 1109 (1960).
- [2] G. Dresselhaus, Spin-orbit coupling effects in zinc blende structures, *Phys. Rev.* **100**, 580 (1955).
- [3] M. I. D'Yakonov and V. I. Perel', Possibility of orienting electron spins with current, *Soviet Journal of Experimental and Theoretical Physics Letters* **13**, 467 (1971).
- [4] J. E. Hirsch, Spin Hall effect, *Phys. Rev. Lett.* **83**, 1834 (1999).
- [5] S. O. Valenzuela and M. Tinkham, Direct electronic measurement of the spin Hall effect, *Nature* **442**, 176 (2006).
- [6] J. C. R. Sánchez, L. Vila, G. Desfonds, S. Gambarelli, J. P. Attané, J. M. De Teresa, C. Magén, and A. Fert, Spin-to-charge conversion using Rashba coupling at the interface between non-magnetic materials, *Nature Communications* **4**, 2944 (2013).
- [7] S. Varotto, A. Johansson, B. Göbel, L. M. Vicente-Arche, S. Mallik, J. Bréhin, R. Salazar, F. Bertran, P. L. Fèvre, N. Bergeal, J. Rault, I. Mertig, and M. Bibes, Direct visualization of Rashba-split bands and spin/orbital-charge interconversion at KTaO_3 interfaces, *Nature Communications* **13**, 6165 (2022).
- [8] A. Soumyanarayanan, N. Reyren, A. Fert, and C. Panagopoulos, Emergent phenomena induced by spin-orbit coupling at surfaces and interfaces, *Nature* **539**, 509 (2016).
- [9] D. Jo, D. Go, G.-M. Choi, and H.-W. Lee, Spintronics meets orbitronics: Emergence of orbital angular momentum in solids, *npj Spintronics* **2**, 19 (2024).
- [10] T. Tanaka, H. Kontani, M. Naito, T. Naito, D. S. Hirashima, K. Yamada, and J. Inoue, Intrinsic spin Hall effect and orbital Hall effect in $4d$ and $5d$ transition metals, *Phys. Rev. B* **77**, 165117 (2008).
- [11] H. Kontani, T. Tanaka, D. S. Hirashima, K. Yamada, and J. Inoue, Giant orbital Hall effect in transition metals: Origin of large spin and anomalous Hall effects, *Phys. Rev. Lett.* **102**, 016601 (2009).
- [12] D. Go, D. Jo, C. Kim, and H.-W. Lee, Intrinsic spin and orbital Hall effects from orbital texture, *Phys. Rev. Lett.* **121**, 086602 (2018).
- [13] T. P. Cysne, S. Bhowal, G. Vignale, and T. G. Rapoport, Orbital Hall effect in bilayer transition metal dichalcogenides: From the intra-atomic approximation to the Bloch states orbital magnetic moment approach, *Phys. Rev. B* **105**, 195421 (2022).
- [14] G. Sala, H. Wang, W. Legrand, and P. Gambardella, Orbital hantle magnetoresistance in a $3d$ transition metal, *Phys. Rev. Lett.* **131**, 156703 (2023).
- [15] I. Lyalin, S. Alikhah, M. Berritta, P. M. Oppeneer, and R. K. Kawakami, Magneto-optical detection of the orbital Hall effect in chromium, *Phys. Rev. Lett.* **131**, 156702 (2023).
- [16] Y.-G. Choi, D. Jo, K.-H. Ko, D. Go, K.-H. Kim, H. G. Park, C. Kim, B.-C. Min, G.-M. Choi, and H.-W. Lee, Observation of the orbital Hall effect in a light metal Ti, *Nature* **619**, 52 (2023).
- [17] T. Yoda, T. Yokoyama, and S. Murakami, Orbital Edelstein effect as a condensed-matter analog of solenoids, *Nano Letters* **18**, 916 (2018).
- [18] A. Johansson, B. Göbel, J. Henk, M. Bibes, and I. Mertig, Spin and orbital edelstein effects in a two-dimensional electron gas: Theory and application to SrTiO_3 interfaces, *Phys. Rev. Res.* **3**, 013275 (2021).
- [19] D. Go, J.-P. Hanke, P. M. Buhl, F. Freimuth, G. Bihlmayer, H.-W. Lee, Y. Mokrousov, and S. Blügel, Toward surface orbitronics: giant orbital magnetism from the orbital rashba effect at the surface of sp-metals, *Scientific Reports* **7**, 46742 (2017).
- [20] L. Salemi, M. Berritta, A. K. Nandy, and P. M. Oppeneer, Orbitaly dominated Rashba-Edelstein effect in noncentrosymmetric antiferromagnets, *Nature Communications* **10**, 5381 (2019).
- [21] L. Chirolli, M. T. Mercaldo, C. Guarcello, F. Giazotto, and M. Cuoco, Colossal orbital Edelstein effect in noncentrosymmetric superconductors, *Phys. Rev. Lett.* **128**, 217703 (2022).
- [22] A. El Hamdi, J.-Y. Chauleau, M. Boselli, C. Thibault, C. Gorini, A. Smogunov, C. Barreteau, S. Gariglio, J.-M. Triscone, and M. Viret, Observation of the orbital inverse Rashba-Edelstein effect, *Nature Physics* **19**, 1855 (2023).
- [23] T. Adamantopoulos, M. Merte, D. Go, F. Freimuth, S. Blügel, and Y. Mokrousov, Orbital Rashba effect as a platform for robust orbital photocurrents, *Phys. Rev. Lett.* **132**, 076901 (2024).
- [24] E. Lesne, Y. G. Sağlam, R. Battilomo, M. T. Mercaldo, T. C. van Thiel, U. Filippozzi, C. Noce, M. Cuoco, G. A. Steele, C. Ortix, and A. D. Caviglia, Designing spin and orbital sources of Berry curvature at oxide interfaces, *Nature Materials* **22**, 576 (2023).
- [25] M. T. Mercaldo, C. Noce, A. D. Caviglia, M. Cuoco, and C. Ortix, Orbital design of Berry curvature: pinch points and giant dipoles induced by crystal fields, *npj Quantum Materials* **8**, 12 (2023).
- [26] K. Ray, S. P. Ananthavel, D. H. Waldeck, and R. Naaman, Asymmetric scattering of polarized electrons by or-

- ganized organic films of chiral molecules, *Science* **283**, 814 (1999).
- [27] R. Naaman, Y. Paltiel, and D. H. Waldeck, Chiral molecules and the electron spin, *Nature Reviews Chemistry* **3**, 250 (2019).
- [28] T. Furukawa, Y. Shimokawa, K. Kobayashi, and T. Itou, Observation of current-induced bulk magnetization in elemental tellurium, *Nature Communications* **8**, 954 (2017).
- [29] F. Calavalle, M. Surez-Rodriguez, B. Martin-Garcia, A. Johansson, D. C. Vaz, H. Yang, I. V. Maznichenko, S. Ostanin, A. Mateo-Alonso, A. Chuvilin, I. Mertig, M. Gobbi, F. Casanova, and L. E. Hueso, Gate-tuneable and chirality-dependent charge-to-spin conversion in tellurium nanowires, *Nature Materials* **21**, 526 (2022).
- [30] S.-H. Yang, R. Naaman, Y. Paltiel, and S. S. P. Parkin, Chiral spintronics, *Nature Reviews Physics* **3**, 328 (2021).
- [31] Y. Liu, J. Xiao, J. Koo, and B. Yan, Chirality-driven topological electronic structure of dna-like materials, *Nature Materials* **20**, 638 (2021).
- [32] S. Han, H.-W. Lee, and K.-W. Kim, Orbital dynamics in centrosymmetric systems, *Phys. Rev. Lett.* **128**, 176601 (2022).
- [33] X. Zhang, Q. Liu, J.-W. Luo, A. J. Freeman, and A. Zunger, Hidden spin polarization in inversion-symmetric bulk crystals, *Nature Physics* **10**, 387 (2014).
- [34] J. M. Riley, F. Mazzola, M. Dendzik, M. Michiardi, T. Takayama, L. Bawden, C. Granerod, M. Leandersson, T. Balasubramanian, M. Hoesch, T. K. Kim, H. Takagi, W. Meevasana, P. Hofmann, M. S. Bahramy, J. W. Wells, and P. D. C. King, Direct observation of spin-polarized bulk bands in an inversion-symmetric semiconductor, *Nature Physics* **10**, 835 (2014).
- [35] A. N. Pal, D. Li, S. Sarkar, S. Chakrabarti, A. Vilan, L. Kronik, A. Smogunov, and O. Tal, Nonmagnetic single-molecule spin-filter based on quantum interference, *Nature Communications* **10**, 5565 (2019).
- [36] In the Supplemental Material we outline the approach for the computation of the examined electron transmission. Additionally, we provide further details on the symmetry properties of the spin and orbital polarization of the transmitted states. We discuss the role of the crystal field potential in the various regions of the transmission system. We discuss the symmetry aspects of the nodal line in the parameters space associated with the orbital moment that is perpendicular to the vector defining the mirror and rotation symmetry breaking.
- [37] Y. Adhikari, T. Liu, H. Wang, Z. Hua, H. Liu, E. Lochner, P. Schlottmann, B. Yan, J. Zhao, and P. Xiong, Interplay of structural chirality, electron spin and topological orbital in chiral molecular spin valves, *Nature Communications* **14**, 5163 (2023).
- [38] J. Gersten, K. Kaasbjerg, and A. Nitzan, Induced spin filtering in electron transmission through chiral molecular layers adsorbed on metals with strong spin-orbit coupling, *The Journal of Chemical Physics* **139**, 114111 (2013).
- [39] H. J. Eckvahl, N. A. Tcyrulnikov, A. Chiesa, J. M. Bradley, R. M. Young, S. Carretta, M. D. Krzyaniak, and M. R. Wasielewski, Direct observation of chirality-induced spin selectivity in electron donor-acceptor molecules, *Science* **382**, 197 (2023).
- [40] P. Streda and P. Seba, Antisymmetric spin filtering in one-dimensional electron systems with uniform spin-orbit coupling, *Phys. Rev. Lett.* **90**, 256601 (2003).